Quaternary Science Reviews 272 (2021) 107222

Contents lists available at ScienceDirect

Quaternary Science Reviews

journal homepage: www.elsevier.com/locate/quascirev

Climatic quantification and seasonality of the late MIS 3 in North China: A perspective from carbon and oxygen isotopes of fossil mammal teeth

Xu Wang [a, b], Jing Sun [c], Fred J. Longstaffe [d], Xuejun Gu [e], Shuisheng Du [f, *], Linlin Cui [a, b], Xiaozhong Huang [g], Zhongli Ding [a, b]

[a] Key Laboratory of Cenozoic Geology and Environment, Institute of Geology and Geophysics, Chinese Academy of Sciences, P.O. Box 9825, Beijing 100029, China
[b] Innovation Academy for Earth Science, CAS, China
[c] The Palace Museum, 4 Jingshan Qianjie, Beijing 100009, China
[d] Department of Earth Sciences, The University of Western Ontario, London, Ontario N6A 5B7, Canada
[e] Luoyang City Cultural Relics and Archaeology Research Institute, Luoyang 471000, China
[f] School of History, Beijing Normal University, 19 Xinjiekouwai Street, Beijing 100875, China
[g] Key Laboratory of Western China's Environmental Systems (Ministry of Education) College of Earth and Environmental Sciences, Lanzhou University, Lanzhou 730000, China

ARTICLE INFO

Article history:
Received 12 July 2021
Received in revised form
24 September 2021
Accepted 1 October 2021
Available online xxx

Handling Editor: Xiaoping Yang

Keywords:
Marine isotope stage 3
North China
Stable isotopes
Fossil mammal tooth
Climate
Seasonality

ABSTRACT

Marine Isotope Stage 3 (MIS 3, at 60–25 ka B.P.) was a short interstadial within the Last Glacial period. A generally warm and wet climatic condition during the MIS 3 period has been suggested by many previous studies. Quantitative climatic reconstruction and studies of seasonality, however, have been seldom attempted given the scarcity of useful proxy indicators. A full understanding the climatic characteristics during this period is hampered by their absence. This is especially the case in the East Asian monsoon region in North China, which is very sensitive to climatic change. To help fill this knowledge gap, we have determined the stable carbon ($\delta^{13}C$) and oxygen isotope ($\delta^{18}O$) compositions of tooth enamel from fossil mammals (*Bubalus* sp [buffalo] and *Cervus elaphus* [red deer], dated at ~33–31 ka B.P.) recovered from Longquan Cave in North China. We use these data to constrain ecology, local air temperature and precipitation amounts during the late MIS 3. The average $\delta^{13}C$ (VPDB) of tooth enamel (−14.4‰ and −8.8‰, respectively for buffalo and red deer) indicate that C_3 plants comprised the main diet of animals living in this area. Pollen assemblages demonstrated that vegetation mainly consisted of grasses and herbs (~64%) with trees only accounting for about 26%. These results indicate a landscape of open steppe with sparsely distributed trees. The reconstructed climate derived from tooth enamel $\delta^{18}O$ was relatively colder and drier than present-day condition, with mean annual air temperature ranging from 4 to 13 °C and mean annual precipitation ranging from 360 to 670 mm. Moreover, the inferred summer and winter half-year temperatures were respectively 8–24 °C and −2 to 5 °C, which represents either similar or weaker seasonality than at the present time. The inferred cold and dry climate suggested by our study contrasts with the warm and wet conditions previously reconstructed using proxy indicators from bulk soil samples in North China. In comparison to the long-term, time-averaged climatic condition reflected by those soil proxies, the stable isotope compositions of fossil more likely recorded climatic conditions at annual or seasonal time-scale. The inferred annual cold/dry climate at Luanchuan Cave suggested by our data may indicate a short climatic cooling event from Greenland Interstadial (GIS) 5 to its following stadial. Mean annual temperature fluctuated by ~8 °C during this interstadial-stadial cycle.

1. Introduction

Marine Isotope Stage 3 (MIS 3), spanning 60–25 ka B.P., was a short interstadial stage within the Last Glacial period (Imbrie et al.,

* Corresponding author.
E-mail addresses: xuking@mail.iggcas.ac.cn (X. Wang), ssdu@bnu.edu.cn (S. Du).

https://doi.org/10.1016/j.quascirev.2021.107222
0277-3791/

1984). The climate during this stage was extremely unstable as reflected in the occurrence of millennial-scale climatic events, i.e., Dansgaard-Oeschger cycles and Heinrich stadials (Dansgaard et al., 1984, 1993; Heinrich, 1988; Johnsen et al., 1992; Stuiver and Grootes, 2000). Previous studies of MIS 3 have mainly focused on regional comparison of millennial-scale climatic variability and the mechanisms causing the abrupt climate events (Sánchez Goñi et al., 2002; Jiménez-Moreno et al., 2010; Sánchez Goñi and Harrison, 2010; Van Meerbeeck et al., 2011; Sionneau et al., 2013; Gibb et al., 2014). Quantitative reconstruction of regional climate (i.e., temperature and precipitation) and study of climate seasonality, however, have seldom been undertaken, in part due to the scarcity of useful proxy indicators or suitable materials to study. This is especially the case for the East Asian monsoon region in North China. This region is ideal for reconstructing paleoclimate and investigating the mechanisms of paleoclimatic evolution because it is more sensitive to abrupt climatic changes and seasonal variations (e.g., Wu et al., 2012).

The carbon ($\delta^{13}C$) and oxygen ($\delta^{18}O$) isotope compositions of tooth enamel (bioapatite) from mammals record information about the food and water consumed by animals (Longinelli, 1984; Bryant et al., 1994; Koch et al., 1998; Wang and Deng, 2005). Tooth enamel is very stable and hence resistant to carbon and oxygen isotope exchange after its formation, particularly during *post-mortem* and diagenetic processes (Quade et al., 1992). Hence, the isotopic information they recorded can directly reflect the climatic and ecological conditions in the study area during the animal's life, including vegetation type, temperature and precipitation (Wang et al., 1994). For example, the $\delta^{18}O$ of bioapatite from fossil tooth enamel has been used to quantitatively reconstruct air temperatures in the geological past (Delgado Huertas et al., 1997; Fricke and O'Neil, 1999; Tütken et al., 2007; Bernard et al., 2009; Amiot et al., 2010; Fabre et al., 2011; Amiot et al., 2011; Amiot et al., 2015). The $\delta^{13}C$ of structure carbonate from fossil tooth enamel has been employed to infer paleodiet and hence ecological information, i.e., the relative abundance of C_3/C_4 vegetation (*e.g.,* Cerling et al., 1997; Koch, 1998; Deng et al., 2002). More recently, the $\delta^{13}C$ of fossil tooth enamel has also been employed to infer paleo-rainfall (Amiot et al., 2015).

In this study, we have determined the carbon and oxygen isotope compositions of bioapatite structural carbonate ($\delta^{13}C_C$ and $\delta^{18}O_C$, respectively) from tooth enamel along the growth bands of fossil teeth of buffalo (*Bubalus* sp.) and red deer (*Cervus elaphus*), excavated from the Longquan Cave Site, Luanchuan County, North China (Fig. 1a). These samples were buried *in situ* at ~33–31 ka B.P. during the late MIS 3 (Du et al., 2016). The oxygen isotope compositions of bioapatite phosphate ($\delta^{18}O_P$) were also measured and compared with the corresponding $\delta^{18}O_C$ to test for preservation of original oxygen isotope signals in the tooth enamel. We then use these data to quantitatively reconstruct temperature and rainfall, with special attention to climatic seasonality at the study site. These results provide insight into the MIS 3 climatic characteristics of North China at ~33–31 ka B.P.

2. Geological setting

Longquan Cave (33°47′24″N, 111°36′28″E) is located in Longquan Mountain Park in Luanchuan County, Luoyang City, Henan province (Fig. 1a). The climate of Luanchuan County is temperate and humid, fitting within the warm temperate continental monsoon climate classification. At present, the mean annual temperature (MAT) at the site is 12 °C, with a summertime (June–August) mean temperature of 22.9 °C and winter (December–February) mean temperature of 0.6 °C. The site's mean annual precipitation is 873 mm, and ~50% of the rainfall occurs in summer, brought by the East Asian summer monsoon (Compilatory Commission of Annals of Luanchuan County, 1994).

Longquan Cave faces east and is situated about 6 m above the modern level of Yihe river. The cave is heavily damaged by erosion and by recent quarrying of its limestone roof and walls. Preserved layers were found at the back of the cave near the southern, western and northern walls. The site was divided into zones A-D and excavated within a grid of 1 m^2 sections (Fig. 1b and c). Zone C had the deepest stratigraphy, followed by zones B, A and D. Deposition in the cave can be subdivided into three stratigraphic layers, as described as below:

Layer 1 is uppermost, consisting of brownish-yellowish clay and brownish-yellowish silty clay, with a thickness of 0.3–1.05 m in zones A and C. In zone D, layer 1 was disturbed by modern human activity and its lower part is brownish-reddish clay with the thickness of only 0.05–0.15 m.

Layer 2 is hard, ~0.5–1.6 m thick and composed of reddish-brown clay, with a few pebbles in some areas. Most of the lithic artefacts and fossil animal bones recovered from the Longquan Cave were in this layer. The lithic assemblage (stone tools) belongs to the core-and-flake industry once prevalent in southern China (Du et al., 2016). The foragers who temporarily camped in the Longquan Cave used the simple core-and-flake technique to obtain flakes with sharp cutting edges. The faunal remains may originate from anthropogenic accumulations. A polished bone tool (i.e., a bone awl) was also discovered in layer 2 from zone D, which marks a significant innovation in tool-making technology. Two hearths were uncovered in layer 2 in zone A at depth of 100 mm and 200 mm, respectively. Collectively, the Longquan Cave provides evidence of traits regarded as similar to other modern human behavior, notably the distinct zoning of domestic areas for specific purposes, the use of hearths and rocks to store thermal energy, and the use of polished bone tools (Du et al., 2016).

Charcoal samples for AMS ^{14}C dating were collected from the upper parts of layer 2 in zones A and D (Fig. 1b). A fossil bone collected from sub-layer 7 of layer 2 in zone D was also dated and had an age of ~33 ka cal BP. A total of eight radiocarbon dates were obtained. These radiocarbon dates were presented by Du et al. (2016), and showed that most of the depositional horizons span ~35 to 31 ka cal B.P. except for the lower hearth, which has a date of ~40 ka cal BP. It is therefore suggested initial human occupation occurred at ~40 ka cal BP, followed by a second period of activity at ~35 to 31 ka cal BP. Hence, the Longquan occupation falls within the MIS 3, a period that was generally marked by relatively rapid climatic fluctuations from colder to warmer on a millennial scale (*e.g.*, Dansgaard et al., 1984, 1993). However, the climatic conditions that facilitated the Longquan occupation of the cave are not known. Since fossil teeth of buffalo and red deer were excavated from the lower part of layer 2 (i.e., sub-layers 5–7), they were assigned to an age of ~33-31 ka cal BP based on the two AMS ^{14}C age control points in Zone D (Fig. 1b). Accordingly, the stable carbon and oxygen isotope compositions of enamel from these fossil tooth samples have been analyzed to help reconstruct the paleoclimate at this time.

Layer 3 is yellowish silt inter-bedded with brown-yellowish clay, and is only exposed in zone C (Fig. 1b). This deposit was excavated to ~0.7 m depth, but few lithics and fossil bones were found.

3. Materials and methods

3.1. Fossil teeth

Five fossil teeth of buffalo and two fossil teeth of red deer were analyzed in this study (Fig. S1). These teeth were visibly well-preserved. The teeth were all excavated from brown-reddish clay

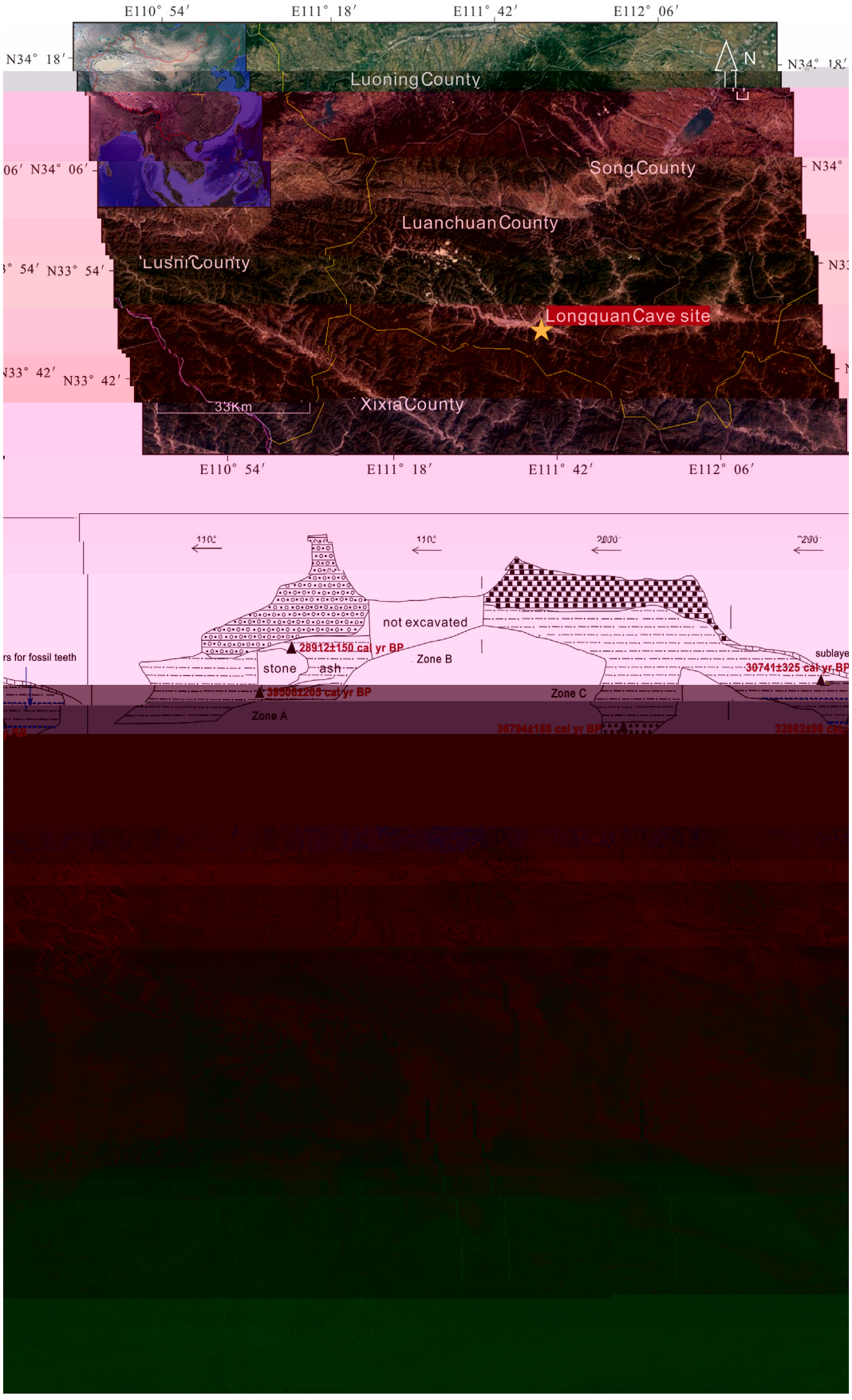
E110° 54′
E111° 18′
E111° 42′
E112° 06′
N34° 18′
N
Luoning County
Song County
Luanchuan County
Lusni County
Longquan Cave site
Xixia County
33Km
N33° 54′
N33° 42′
not excavated
Zone A
Zone B
Zone C
stone
ash
28912±150 cal yr BP
sublaye
30741±325 cal yr BP

in the layer 2, with six of them from sub-layers 5, 6 and 7 in zone D and one of them from sub-layer 5 in zone A (Table 1). Specifically, LCMD2(5):34 and LCMD2(6):19 are the third molar teeth (M3) from the upper jaws of two individual red deer collected from the sub-layer 5 and 6 of layer 2 in zone D, respectively. Tooth LCMA2(5):66−3 is the fourth deciduous premolar from the lower jaw of a buffalo, excavated from sub-layer 5 of layer 2 in zone A. Sample LCMD2(5):16 consists of three sequential molar teeth M1, M2 and M3 from the upper jaw of a buffalo unearthed from sub-layer 5 of the layer 2 in zone D. LCMD2(7):23−2 is the second molar tooth (M2) from the upper jaw of a buffalo, which was excavated from sub-layer 7 of layer 2 in zone D.

The samples described above belong to different tooth types, which would have had different formation times and growth rates. Intra-tooth isotopic analysis can therefore provide a wealth of information about seasonal changes over the period of tooth enamel development. For example, *C. elaphus* third molars (M3) erupt between 21 and 32 months, with enamel mineralization proceeded between 9 and 26 months (Godawa, 1989; Brown and Chapman, 1991; Azorit et al., 2002). Since deer calves are born in spring, the time sequence recorded in the M3 should therefore span early spring/summer/autumn/winter/late spring (Stevens et al., 2011).

The tooth formation sequence of *Bubalus* sp. is assumed to be similar to that of modern bison (Gadbury et al., 2000; Fricke and O'Neil, 1996). This sequence starts with growth of M1 *in utero* at the end of winter, followed by mineralization of M2 during the first year of the animal's life (summer to summer), then by M3, P2, P3 and P4 during the next year (Bernard et al., 2009). In this case, sample LCMD2(5):16, which contained M1, M2 and M3 in sequence, may represent a continuous record of the $\delta^{13}C$ and $\delta^{18}O$ of diet and drinking water for a period of at least two years. The other samples (*e.g.*, M2 and P4) probably documented one year's variation in isotopic compositions. We note, however, that the first molar (M1) forms, at least in part, *in vitro* from the body water of the mother. Hence, its $\delta^{18}O$ is unlikely to reflect the value of local meteoric water (Fricke and O'Neil, 1996). The second molar (M2) may start to form prior to weaning and its $\delta^{18}O$ may be slightly affected by isotopic composition of the milk the calf consumed during nursing (Gadbury et al., 2000).

3.2. Sampling

The teeth were fi

Table 1
Mean stable carbon and oxygen isotope results for tooth enamel from red deer (*Cervus elaphus*) and buffalo (*Bubalus* sp.).

Sample No.	Horizon	Species	Tooth type	$\delta^{13}C_C$ (‰, VPDB)	$\delta^{18}O_C$ (‰, VSMOW)	Number of $\delta^{13}C_C/\delta^{18}O_C$ microsamples (n)	$\delta^{18}O_P$ (‰, VSMOW)	Number of $\delta^{18}O_P$ microsamples (n)	$\delta^{18}O_C$ - $\delta^{18}O_P$ (‰)
LCMD2(5):34	2(5)	*Cervus elaphus*	[a]UP M3	−13.2	+23.2	17	+13.9	8	9.3
LCMD2(6):19	2(6)	*Cervus elaphus*	UP M3	−12.9	+23.9	11	+16.1	5	7.8
LCMA2(5):56-3	2(5)	*Bubalus* sp.	LR dP4	−13.5	+23.5	14	+13.3	13	10.2
LCMD2(5):16	2(5)	*Bubalus* sp.	UP M1	−13.2	+20.4	9	+11.9	9	8.4
			UP M2	−13.1	+20.4	11	+12.9	13	7.5
			UP M3	−13.1	+19.3	9	+12.5	12	6.8
LCMD2(7):23-2	2(7)	*Bubalus* sp.	UP M2	−10.3	+22.4	34	+16.6	32	5.8

Each isotopic result is the calculated mean for whole-tooth enamel from several microsamples (*n*). Individual data are tabulated in Supplementary Table S1.
[a] LR and UP represent lower and upper jaw, respectively; M denotes molar tooth and dP denotes deciduous premolar.

and $\delta^{18}O_C$ for this standard was better than ±0.1‰ and ±0.2‰ (1SD, n = 10), respectively. We also performed duplicate analyses of ten enamel sub-samples to determine their isotopic reproducibility. The maximum difference between duplicate enamel analyses was 0.2‰ for $\delta^{13}C$ and 0.25‰ for $\delta^{18}O$. The oxygen isotope compositions were then converted from the VPDB scale to the VSMOW scale using the equation: $\delta^{18}O_{VSMOW} = 1.03091 \times \delta^{18}O_{VPDB} + 30.91$ (Coplen et al., 1983).

Extraction of bioapatite phosphate consists of isolating the phosphate anionic complexes using acid dissolution and anion-exchange resin and its precipitation as silver phosphate, according to a protocol reported by Crowson et al. (1991) and slightly modified by Lécuyer et al. (1993). Silver phosphate was quantitatively precipitated in a thermostatic bath set at 70 °C. The silver phosphate was then recovered by filtration, washing with double-deionised water, and then drying at 50 °C. Extraction of bioapatite phosphate from one buffalo tooth (LCMD2(7):23−2) was carried out at LEIG-IGGCAS and its $\delta^{18}O_P$ measured using a high temperature conversion elemental analyzer (TC/EA) linked to MAT253 isotope ratio mass spectrometer (Thermo Scientific™). Extraction and isotopic analysis of bioapatite phosphate from the other six fossil teeth were performed at the Laboratory for Stable Isotope Science, *The* University *of* Western Ontario, Canada (LSIS UWO). The $\delta^{18}O_P$ of those silver phosphate subsamples were measured using a TC/EA coupled with a Delta™ Plus XL isotope ratio mass spectrometer (Thermo Scientific™).

Values of $\delta^{18}O_P$ are reported relative to VSMOW, as calibrated using IAEA-CH-6 ($\delta^{18}O = +36.4$‰; Flanagan and Farquhar, 2014) and Aldrich Silver Phosphate−98%, Batch 03610 EH ($\delta^{18}O = +11.2$‰; Webb et al., 2014). Silver phosphate precipitated from standard NBS120c (Miocene phosphorite from Florida: $\delta^{18}O_P = +21.7$; Amiot et al., 2011) was analyzed along with the silver phosphate samples derived from the fossil teeth as a check on the calibration. The reproducibility of $\delta^{18}O$ results for standards (Aldrich, n = 18; IAEA-CH-6, n = 10; NBS120c, n = 5) and duplicate sample pairs (n = 18) was better than ±0.3‰ (SD) in all cases.

3.4. Pollen analysis

A total of eight soil samples were collected from Longquan Cave section for pollen analysis. The samples were processed using standard methods, including treatment with HCl (10%), hot KOH (10%) for 5−10 min, HF (64%), and fine sieving in an ultrasonic bath (Faegri et al., 1989). At the beginning of the procedure one tablet of *Lycopodium* spores was added to each sample to enable calculation of the pollen concentration (Maher, 1981). The pollen concentrates were mounted in glycerol and examined at × 400 magnification using a Nikon optical microscope (Model: ECLIPSE-80i). Where appropriate, magnifications of × 600 and/or × 1000 were used to examine pollen surface sculpturing. Identification was aided by reference to Wang et al. (1995), together with comparisons with modern pollen reference collections. Pollen counts consisted of ~200−400 terrestrial pollen grains except for two samples at lower part of the sequence where the pollen abundance was much lower. Pollen percentages were calculated based on the sum of all terrestrial pollen taxa present.

4. Results

All stable isotope data ($\delta^{13}C_C$, $\delta^{18}O_C$ and $\delta^{18}O_P$) for each tooth are listed in Table S1. Fig. 2 illustrates changes in $\delta^{13}C_C$ (VPDB) and $\delta^{18}O_C$ (VSMOW) along the growth axis of each tooth. For the two fossil teeth of red deer, $\delta^{13}C_C$ ranges from −13.5 to −12.4‰ and $\delta^{18}O_C$ ranges from +22.2 to +24.5‰. Neither tooth for the red deer recorded a full range of seasonal changes in isotopic composition, possibly because the teeth were relatively short (<20 mm) and the crowns were partially worn.

Larger variations are observed for $\delta^{13}C_C$ (−14.3 to −8.8‰) and $\delta^{18}O_C$ (+17.6 to +25.1‰) of the five fossil buffalo teeth. These variations can be attributed to seasonal changes. Tooth LCMA2(5):56−3 is a deciduous premolar and documented a half cycle of seasonal changes in its $\delta^{18}O_C$ and $\delta^{13}C_C$. By comparison, tooth LCMD2(7):23-2 measures ~70 mm from cervix to apex and its $\delta^{18}O_C$ exhibits a sinusoidal pattern of variation attributed to a full seasonal cycle. By contrast, the $\delta^{13}C_C$ of this tooth showed more frequent fluctuations about −10.3‰. Sample LCMD2(5):16 contained 3 M teeth from the first to the third molar (designated as LCMD2(5):16 M1, LCMD2(5):16 M2 and LCMD2(5):16 M3, respectively). Their isotopic data can be combined to generate a composite isotopic seasonal time series. Because the M1 tooth of cattle is known to form prior to birth (Fricke and O'Neil, 1996), it must have formed *in vitro* from the body water of mother. We assume that the same tooth eruption schedule holds for its close relative, the buffalo. Therefore, its M1 tooth can be used to investigate seasonality during the birthing period, followed by the M2 and M3 whose isotopic data provide a good illustration of seasonal variations (Fig. 2).

Fig. 3 compares intra-tooth variation in $\delta^{18}O_P$ and $\delta^{18}O_C$ for each fossil tooth. Overall, $\delta^{18}O_P$ generally describes the same pattern as $\delta^{18}O_C$. The $\delta^{18}O_P$ for the two red deer teeth range from +12.6 to +14.4‰ for LCMD2(5):34 and from +13.9 to +19.3‰ for LCMD2(6):19. The latter tooth displays a sharp decrease in $\delta^{18}O_P$ from the apex towards the cervix, a pattern also observed for $\delta^{18}O_C$.

The $\delta^{18}O_P$ of the LCMA2(5):56−3 pre-molar buffalo tooth (dP4)

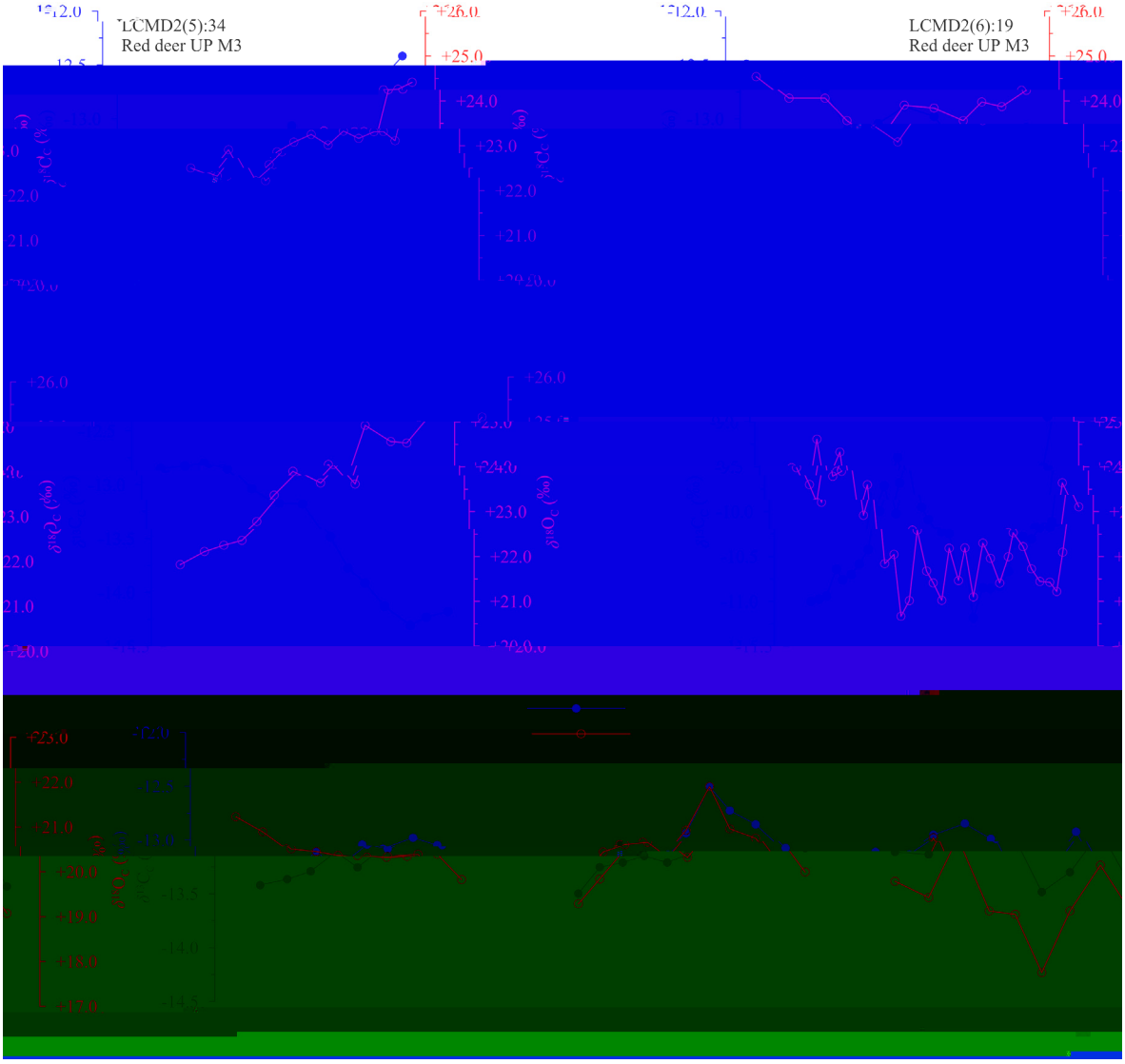

Fig. 2. Intra-tooth variations in stable carbon and oxygen isotope compositions of bioapatite structural carbonate ($\delta^{13}C_C$ in ‰, VPDB; $\delta^{18}O_C$ in ‰, VSMOW) in tooth enamel of seven fossil teeth versus distance (in mm) from the cervix.

fluctuates widely (+11.9 to +14.8‰), while increasing overall with decreasing distance from the cervix. The $\delta^{18}O_P$ for the long buffalo tooth LCMD2(7):23-2 shows a much more restricted range (+15.7 to +17.2‰; mean = +16.6‰). Its narrow range of $\delta^{18}O_P$ nevertheless registers a full seasonal cycle of variation. The molar (M1~M3) teeth set of LCMD2(5):16 show a larger oscillation in $\delta^{18}O_P$ from +10.6 to +17.9‰, which is suggestive of seasonal variation. The M1 has very low $\delta^{18}O_P$ showing little variation (+11.3 to +12.5‰), the M2 shows the largest variation in $\delta^{18}O_P$ (+10.6 to +17.9‰), rising to maximum values near its center, followed by a large decrease, and the M3 exhibits a gradual decrease from +13.6 to +10.7‰.

Table 1 lists mean values of $\delta^{13}C_C$, $\delta^{18}O_C$ and $\delta^{18}O_P$ for each tooth. The mean $\delta^{13}C_C$ varies from −13.5 to −12.9‰, except one more positive value of −10.3‰ (buffalo tooth LCMD2(7):23−2). The mean $\delta^{18}O_C$ varies from +19.3 to +23.9‰. The mean $\delta^{18}O_P$ ranges from +11.9 to +16.6‰. The mean value of $\delta^{18}O_C$ - $\delta^{18}O_P$ varies from +5.8 to +10.2‰, with no apparent inter-species differences.

The pollen samples were composed of 22 plant species, mainly trees, shrubs, grasses and herbs, and a few ferns (Fig. 4). Trees consisted of spruce (*Picea*), birch (*Betula*), elm (*Ulmus*), willow (*Salix*), cypress (*Cupressaceae*) and a small quantity of poplar/aspen/cottonwood (*Populus*) and comprise ~27% of the pollen count. Shrubs included *Elaeagnaceae*, *Ephedra* and *Rosaceae*, but account for only ~3% of the pollen count. Of the grasses and herbs, *Ranunculaceae* and *Gramineae* most frequently occurred, with sporadic emergence of *Chenopodiaceae*, *Artemisia*, *Cypereceae*, *Compositae*, *Leguminoceae*, and *Typha*. The grasses and herbs comprise ~64% of the pollen count. Spores make up ~6% of the pollen count.

5. Discussion

5.1. Factors influencing stable carbon and oxygen isotope compositions of mammalian tooth enamel

For herbivores like red deer and buffalo, their tooth enamel $\delta^{13}C_C$ is generally governed by the carbon isotope compositions of their plant forage. Most modern plants photosynthesize using either the C_3 pathway (C_3 plants) or the C_4 pathway (C_4 plants). Modern C_3 plants, which include trees, most shrubs and cool season

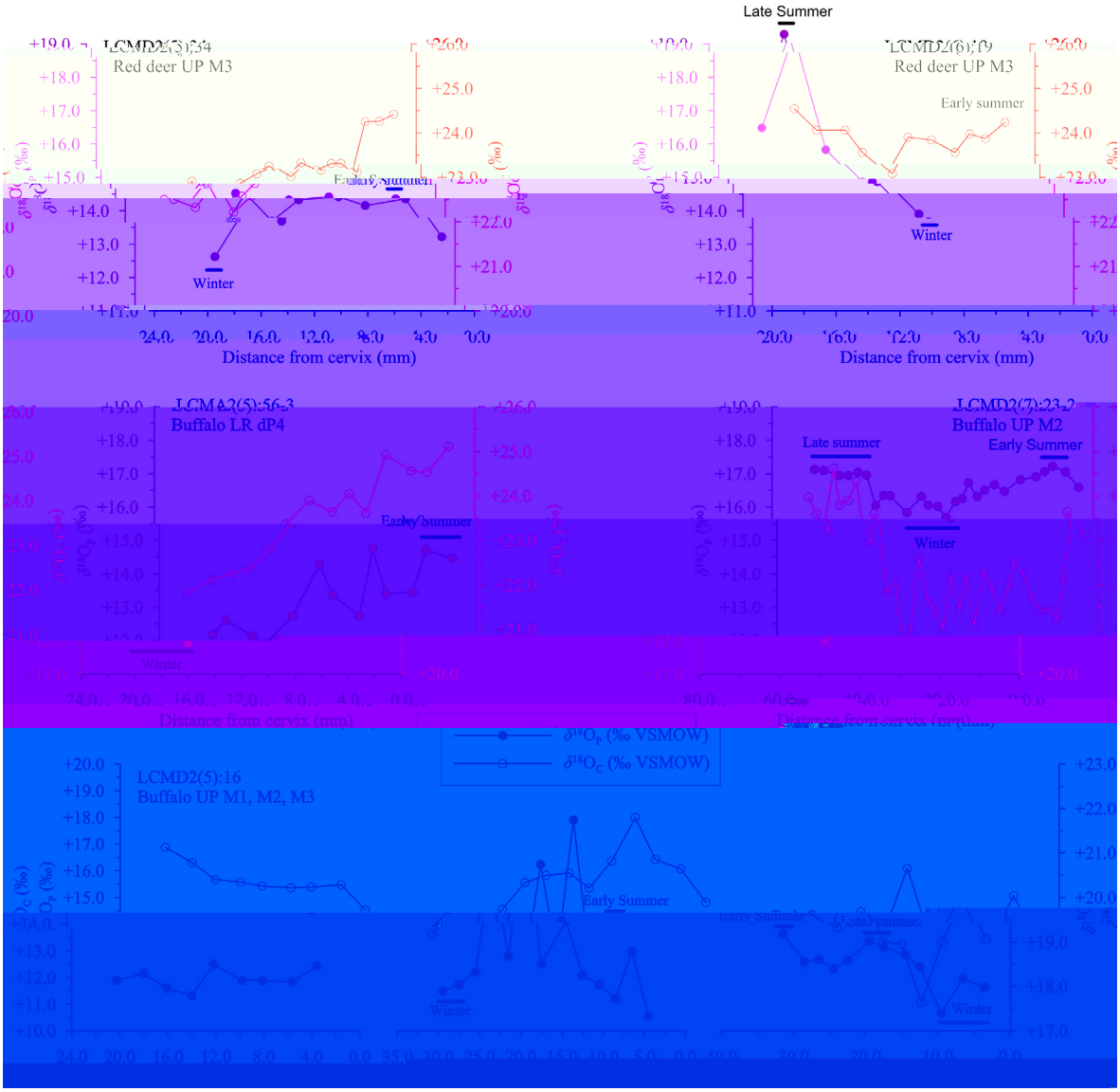

Fig. 3. Intra-tooth variations in oxygen isotope compositions of bioapatite phosphate ($\delta^{18}O_P$ in ‰, VSMOW), compared to data for bioapatite structural carbonate ($\delta^{18}O_C$ in ‰, VSMOW) in tooth enamel of seven fossil teeth. The $\delta^{18}O_P$ and $\delta^{18}O_C$ show generally similar changing patterns in the same tooth. Seasons were assigned according to the peaks and troughs of $\delta^{18}O_P$ and $\delta^{18}O_C$ curves, as shown by horizontal bars.

grasses, have $\delta^{13}C$ ranging from about −35 to −20‰, with an average of −27‰ (O'Leary, 1981; O'Leary, 1988; Farquhar et al., 1989). By contrast, modern C_4 plants, which are mostly warm season grasses, have $\delta^{13}C$ ranging from about −17 to −9‰, averaging −13‰. These isotopic signals are passed along the food chain to animal tissues with further isotopic fractionation. The average carbon isotope fractionation factor between bioapatite structural carbonate and diet is ~14‰ for ungulate mammals (Cerling and Harris, 1999; Passey et al., 2005). Therefore, a $\delta^{13}C_C$ of −13‰ would ideally indicate a dietary intake of modern pure C_3 plants whereas a $\delta^{13}C_C$ of +1‰ would indicate a pure diet of modern C_4 vegetation (e.g., Wang et al., 2008). This provides a guideline for inferring the proportions of C_3 and C_4 plants in a herbivore's diet, as has been done in many previous studies (e.g., MacFadden et al., 1996; Cerling et al., 1997; Wang and Deng, 2005). Other factors, however, such as soil moisture, aridity and atmospheric pCO_2 can induce a large variability (up to several per mil) in the $\delta^{13}C$ of plants (e.g., Farquhar et al., 1989; Cerling et al., 1997), which need to be considered when inferring the C_3/C_4 from $\delta^{13}C_C$. In addition, because of the Suess Effect (*e.g.*, Keeling, 1979; Marino et al., 1992), the ranges and averages of vegetation $\delta^{13}C_{,\text{ and}}$ therefore $\delta^{13}C_C$, would have been higher by ~1.5–2‰ during MIS 3, *i.e.*, −11.5‰ and +2.5‰ for teeth of mammals ingesting pure C_3 and C_4 plants, respectively.

The oxygen isotope composition of tooth enamel in mammals is directly linked to the $\delta^{18}O$ of body water because mammalian tooth bioapatite is formed at constant body temperature (Longinelli, 1984; Luz et al., 1984; Iacumin et al., 1996). Body water $\delta^{18}O$ is controlled by several factors, including the $\delta^{18}O$ of drinking water and water in food (i.e., plants for herbivores), physiological processes and dietary or drinking behavior (Longinelli, 1984; Luz et al., 1984; Kohn et al., 1996). Several studies have shown that the $\delta^{18}O$ signal in tooth enamel from large animals (>1 kg) is dominated by meteoric water (mw) because most ingested water comes from that source (Longinelli, 1984; Luz et al., 1984; Bryant et al., 1996). Because $\delta^{18}O_{mw}$ correlates with climatic variables including

temperature, seasonality of rainfall and rainfall amount (Dansgaard, 1964; Rozanski et al., 1993), the $\delta^{18}O$ of enamel can be used to reconstruct paleoclimatic conditions during tooth growth (e.g., Longinelli, 1984; Bryant et al., 1994; Bryant et al., 1996; Wang et al., 2008). The most common application of this $\delta^{18}O_C$ and $\delta^{18}O_P$ proxy has been to infer local surface temperatures in the geological past (*e.g.*, Delgado Huertas et al., 1997; Fricke and O'Neil, 1999; Wang and Deng, 2005; Tütken et al., 2007; Bernard et al., 2009; Amiot et al., 2010; Fabre et al., 2011; Amiot et al., 2011; Amiot et al., 2015).

Another significant use of tooth enamel $\delta^{13}C_C$ and $\delta^{18}O_C/\delta^{18}O_P$ has been to trace seasonal variations in diet and climate during tooth growth through analysis of serial enamel samples from an individual tooth (e.g., Fricke and O'Neil, 1996; Dettman et al., 2001; Bernard et al., 2009; van Dam and Reichart, 2009; Metcalfe et al., 2011). This approach is undertaken because mammalian tooth enamel forms incrementally from the crown to the cervix of the tooth, recording a series of $\delta^{13}C_C$ and $\delta^{18}O_C/\delta^{18}O_P$ over time. These isotopic compositions may vary by several per mil along the growth axis within a single tooth and thus provide an excellent record of dietary and/or climatic seasonality, albeit that the isotopic signal might be attenuated due to the time-averaging effect induced by the sampling technique (Passey and Cerling, 2002), as discussed earlier. Migratory behavior can also make seasonal inferences from such isotopic data more complicated. Red deer, however, are not a migratory species (Fabre et al., 2011) and their tooth $\delta^{18}O$ has been shown to record perfect seasonal variation (Stevens et al., 2011). In contrast, the migratory behavior of the Chinese buffalo is not fully known. Because buffalo is water-dependent animal, it relies mostly on standing water sources (e.g., lakes). The Yihe River, which is located nearby our study area, likely met this demand, thus minimizing demands on the buffalo to travel long distances. In addition, the aquatic plants associated with the river system may have offered preferred forage to the buffalo.

5.2. Carbon isotopes, paleodiet and paleoecology at the study site

The intra-tooth

vegetation-dominated environment in this region could vary from dense forest to steppe with sparse trees. The range of carbon isotope compositions calculated here (range: −29.1 to −23.6‰) is more typical of a steppe environment. Dense forest vegetation typically has more negative $\delta^{13}C$ (as low as −34‰) due to the influence of soil respiration associated with the canopy effect (Schleser and Jayasekera, 1985; Sternberg et al., 1989; Van der Merwe and Medin, 1989; Drucker et al., 2008; Bonafini et al., 2013).

The possibility of a steppe-like environment is confirmed by the pollen data for our study site (Fig. 4). Grasses and herbs comprised the majority (~64%) of the pollen count, whereas trees and shrubs were in a distinct minority (~30%). Collectively, the pollen data indicate an open steppe landscape with a sparse distribution of trees, suggestive of a relatively cold and dry climate (*e.g.*, Jiang and Ding, 2005). The inferred landscape is in accordance to red deer's preferred ecological niche, red deer like a boreal forest-meadow habitat, including alpine forest, shrub and grassland environments (Zhao, 1974).

5.3. Climate reconstruction and seasonality in North China during the late MIS 3

5.3.1. Tooth enamel $\delta^{13}C_C$ and paleorainfall reconstruction

Water availability is an important factor that influences plant carbon isotope discrimination in plants (Deines, 1980; Francey and Farquhar, 1982). A restricted soil water supply causes plants to close their stomata to conserve water for photosynthesis. This process in turn reduces the intercellular partial pressure of CO_2, which causes plant $\delta^{13}C$ to rise accordingly. Recent investigations of modern ecosystems in northern China have shown that plant $\delta^{13}C$ shifts toward more negative values with an increase in mean annual precipitation (MAP) (Wang et al., 2003, 2013a; Liu et al., 2005). Wang et al. (2003), for example, observed a 0.47‰ negative shift in $\delta^{13}C$ of C_3 plants with an annual 100 mm increase in rainfall. Several recent studies have used such correlations to infer precipitation amount from the $\delta^{13}C$ of C_3 plants (e.g., Wang et al., 2013a; Amiot et al., 2015).

We initially attempted to adopt a previously established relationship between local MAP and the carbon isotope composition of modern C_3 plants in North China (Wang et al., 2013a) to estimate local precipitations at our study site. However, a recent study has shown that there is a strong positive correlation between the $\delta^{13}C$ of C_3 plants and mean annual temperature in north China (0.104‰ per °C; Wang et al., 2013b). We have corrected for this effect, after removal of two outliers from the Wang et al. (2013a) dataset, to obtain the following regression (Fig. 5):

$$MAP = 90.862(\pm 14.050) \times \Delta_{leaf} - 1360.154(\pm 270.574)\ (R^2 = 0.59) \quad (1)$$

where $\Delta_{leaf} = (\delta^{13}C_{atm} - \delta^{13}C_{leaf})/(1 + \delta^{13}C_{leaf}/10^3)$, $\delta^{13}C_{atm}$ is $\delta^{13}C$ of atmospheric CO_2, and $\delta^{13}C_{leaf}$ represents the C_3 plant $\delta^{13}C$ corrected for the temperature effect.

Average local precipitation amounts calculated using equation (1) are listed in Table 2, using $\delta^{13}C_{atm} = -6.6$‰, as estimated for the late MIS 3 bases on CO_2 trapped in EPICA Dome C ice core (Lourantou et al., 2010), and the calculated mean $\delta^{13}C$ of fossil tooth enamel. All calculated values for our study site are below 670 ± 169 mm, with most of them ranging between 590 and 670 mm. Despite that the first molar (M1) of buffalo sample LCMD2(5):16 was formed *in utero* and the second molar (M2) was partly subject to nursing effects, their $\delta^{13}C$ generate MAP of 639 ± 161 mm and 627 ± 158 mm, respectively, very close to that obtained from the third molar (M3: 633 ± 160 mm). Moreover, the $\delta^{13}C$ for teeth of both red deer and buffalo from the sub-layer 5 yield a consistent MAP of ~630 mm (Table 2). A comparable MAP (596 ± 150 mm) was also determined for red deer tooth (LCMD2(6):19) collected in sub-layer 6. However, the MAP inferred from buffalo tooth LCMD2(7):23−2 collected in the sub-layer 7 was substantially lower (363 ± 91 mm). This may reveal highly variable fluctuations in precipitation amounts at different times during late MIS 3. Collectively, inferred MAP are lower than the average annual amount of modern precipitation (873 mm). This relatively dry condition is consistent with the development of open steppe in the region, as also suggested by the pollen assemblages.

5.3.2. Tooth enamel $\delta^{18}O_P$ and paleotemperature reconstruction

As discussed earlier, $\delta^{18}O_P$ and $\delta^{18}O_C$ of mammal teeth are ultimately controlled by $\delta^{18}O_{mw}$ (*e.g.*, Cormie et al., 1994; Kohn et al., 1996; Kohn and Cerling, 2002; Straight et al., 2004). In the current study, $\delta^{18}O_{mw}$ has been estimated from the $\delta^{18}O_P$ using various phosphate oxygen isotope-water geothermometers. In the absence of a buffalo-specific equation, the bison bioapatite enamel-water geothermometer of Bernard et al. (2009), following Hoppe (2006), was used, recognizing that buffalo and bison have similar body size and physiology:

$$\delta^{18}O_{mw} = 1.18(\pm 0.07) \times \delta^{18}O_P - 27.2(\pm 1.1)\ (R^2 = 0.8) \quad (2)$$

An oxygen isotope bioapatite enamel-water geothermometer for red deer was developed based on the data of D'Angela and Longinelli (1990):

$$\delta^{18}O_{mw} = 0.879(\pm 0.033) \times \delta^{18}O_P - 22.50(\pm 0.52)\ (R^2 = 0.99) \quad (3)$$

Amiot et al. (2004) developed a transfer function of $\delta^{18}O_{mw}$ to mean annual air temperature (MAT) by analyzing the monthly averages of temperature and isotopic data provided by the global network of stations operated by the IAEA–WMO (International Atomic Energy Agency–World Meteorological Organization):

$$\delta^{18}O_{mw} = 0.49(\pm 0.03) \times MAT\text{-}14.18(\pm 0.52)\ (R^2 = 0.81) \quad (4)$$

Using equations (2)/(3) and (4), the calculated MAT at our study site ranged from 2.2 ± 0.9 °C to 13.3 ± 1.2 °C during this portion of MIS 3 (Table 2). The lowest MAT value, however, was calculated for the $\delta^{18}O_P$ of the M1 tooth, which was influenced by the mother body fluid and therefore is disregarded. The remaining range (3.4 ± 0.9 to 13.3 ± 1.2 °C) still represents a very large inter-annual variation in MAT. While the errors overlap, the mean MAT of 7.7 ± 4.0 (1SD) °C is likely diagnostic of temperatures lower than the present-day annual value of ~12 °C.

The seasonality of air temperatures (T_{air}) at Longquan Cave site during the late MIS 3 can perhaps be better estimated using linear regression equations of $\delta^{18}O_{mw}$-T_{air} derived from data obtained closer to the study area rather than from average values inferred from global datasets. We calculated such annual and seasonal regressions using a sub-dataset (1985–2003) for stations in China available through the IAEA-GNIP/ISOHIS dataset (World Data Center for Paleoclimatology, 2006) (Fig. 6a). Four stations were excluded, however, either due to a strong, year-round amount effect (Guangzhou, Haikou and Hongkong) or altitude effect (Lasha). Their exclusion improved the $\delta^{18}O_{mw}$-T correlation.

The annual and winter regression equations obtained were:

Annual:

$$\delta^{18}O_{mw} = 4.765(\pm 0.548) \times \ln(MAT) - 19.578(\pm 1.362)\ (R^2 = 0.75) \quad (5)$$

Winter half-year (October–March):

$$\delta^{18}O_{mw} = 0.681(\pm 0.052)T_{air} - 12.689(\pm 0.407)\ (R^2 = 0.87) \quad (6)$$

There was no significant correlation of $\delta^{18}O_{mw}$ with summer T_{air}, likely because of an apparent amount effect that produced a lowering of $\delta^{18}O_{mw}$ in the summer period. This effect is illustrated in Fig. 6b for Zhengzhou City, which is located close to the study area. Summer temperature (half year: April to September) was therefore calculated from using the inferred winter half-year T_{air}

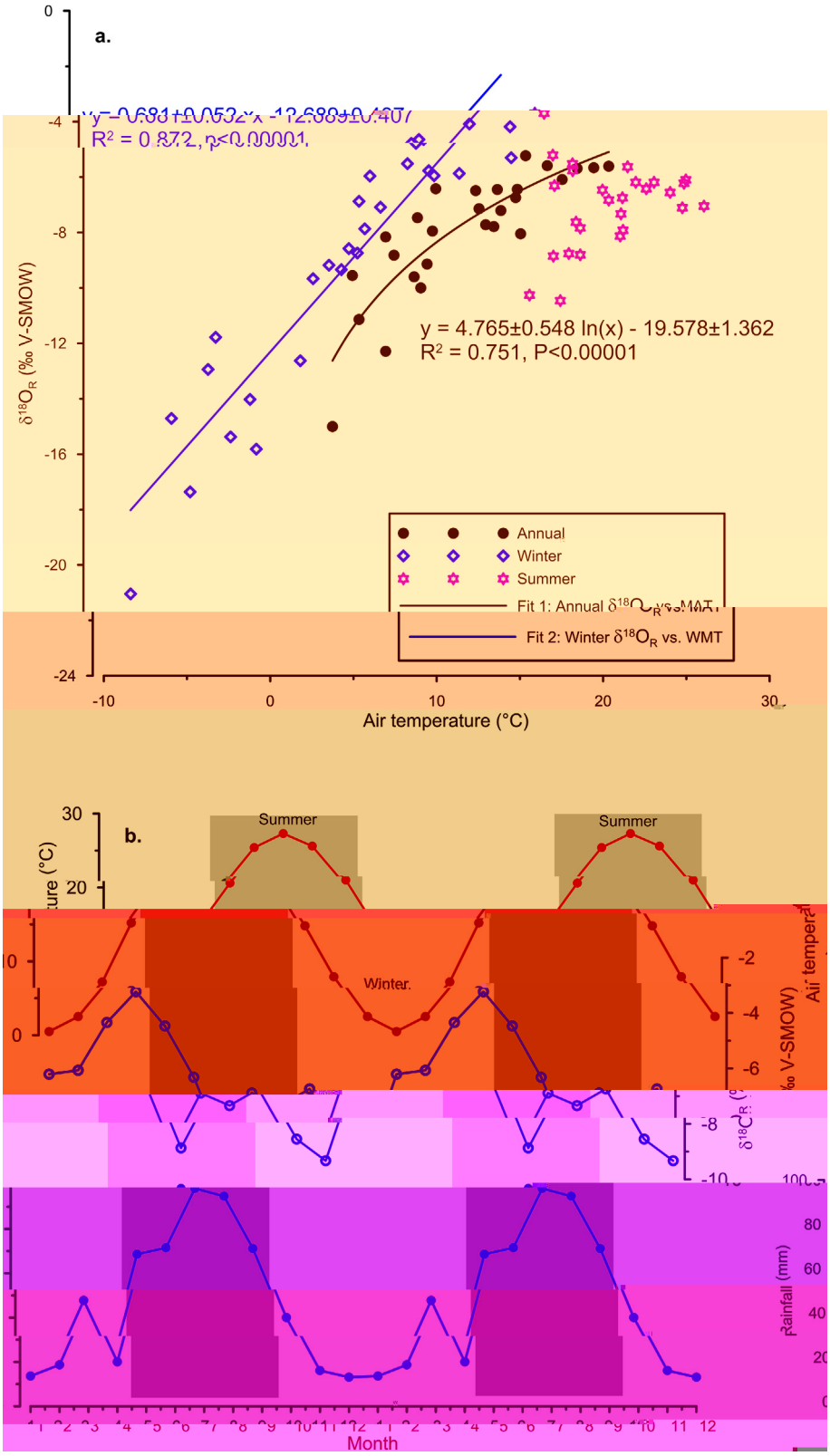

Fig. 6. (a) Monthly variations in air temperature (° C), rainfall $\delta^{18}O$ (‰, VSMOW) and rainfall amount (mm) in Zhengzhou city (~250 km from Luanchuan County). There is a negative shift in the $\delta^{18}O$ of precipitation during summer months (May–September) because of the rainfall amount effect. (b) Correlation of rainfall $\delta^{18}O$ with annual temperature, summer (April–September) and winter (October–March) temperatures. There is no significant correlation of rainfall $\delta^{18}O$ with summer half-year temperature due to the rainfall amount effect.

for modern buffalo from the Shunshanji archaeological site (33°34′58″N, 118°10′8″E) in Sihong County (Tian et al., 2013), which is located 700 km to the east. In that study, $\delta^{13}C_c$ and $\delta^{18}O_c$ were measured for ten subsamples taken from a premolar tooth at an interval of 5 mm along a growth band. The $\delta^{13}C_c$ values (−2.5 to −4.7‰) indicated that the buffalo had ingested a substantial amount of C_4 plants (Tian et al., 2013). As such, these results are unfortunately not suitable for rainfall reconstruction. The $\delta^{18}O_c$ values, however, showed typical seasonal variation (Fig. S2) and were used to estimate MAT, winter half-year and summer half-year temperatures. Before temperature reconstruction, $\delta^{18}O_c$ was translated to $\delta^{18}O_p$ using the average $\delta^{18}O_c$-$\delta^{18}O_p$ offset (7.7‰) for buffalo obtained in our study (Table 1). The reconstructed MAT using equation (4) is 13.0 °C (Table S2), which is comparable to the present mean annual temperature of 14.6 °C at that site. The inferred winter half-year temperature is 4.0 °C, which is ~2 °C lower than measured directly. The inferred summer half-year temperature of 22.1 °C is very close to the measured value (22.9 °C) (Table S2). The general comparability between the inferred and measured temperatures provides a measure for the reliability of the temperature equations presented here. The negative offset of ~2 °C for the inferred temperatures provides a useful reference when comparing inferred paleotemperatures with present temperatures at our study site.

The winter and summer $\delta^{18}O_P$, reconstructed $\delta^{18}O_{mw}$ and resulting average seasonal temperatures are listed in Table 3. The reconstructed winter (October–March) half-year temperatures varied from −2.5 ± 0.8 °C to 5.3 ± 0.7 °C (mean: 0 ± 3 (1SD) °C), with the general condition being lower than the present temperature of ~5 °C during the same months, notwithstanding the ~2 °C offset observed for the winter temperature reconstruction using the modern buffalo tooth enamel. The inferred summer (April–September) temperatures showed a large range of variation from 8.4 ± 1.3 to 23.6 ± 1.2 °C (mean: 15 ± 6 (1SD) °C). The inferred mean summer temperature is below the present average summer temperature of ~20 °C for the same period in Luanchuan County.

If we examine the temperature data by sub-layer, a possible reason for the large variations becomes apparent. The inferred MAT, winter and summer temperatures for sub-layers 6 and 7 were 11.3 °C and 13.2 °C, 0 °C and 5.3 °C, and 23.6 °C and 21.3 °C, respectively. In contrast, the inferred MAT, winter and summer temperatures for sub-layer 5 were 3.4 °C to 7.9 °C, −2.5 °C to 0.7 °C, and 8.4 °C–15.1 °C, respectively. The inferred temperatures for sub-layers 6 and 7 are much higher than those for sub-layer 5. Moreover, the inferred temperatures show a decreasing trend from sub-layer 7 to 5. Assuming a normal age-depth model, this change may represent a transition from interstadial to stadial mode, possibly Greenland Interstadial (GIS) 5 to its following stadial during ~33-31 cal ka BP as recorded in the $\delta^{18}O$ records of Chinese stalagmites and the GISP2 ice core (Wang et al., 2001). If so, GIS 5 had temperature conditions similar to today whereas the stadial was characterized by a mean annual temperature drop of ~8 °C. Our calculations also suggest that the climatic seasonality in Luanchuan County during the late MS 3 was variable, i.e., GIS 5 possessed a seasonality similar to present-day whereas the stadial had weaker seasonality than today.

5.4. Late MIS 3 paleoclimate estimates using different proxies in North China

Only a few previous studies have attempted to quantify paleoclimatic during the MIS 3 in North China. Li et al. (2011) reconstructed climatic change in Tangshan over the last 200 ka using a pollen-climate transfer function; the inferred MAT and MAP during 40–20 ka B.P. were lower by 5 °C and 150 mm, respectively, than present conditions. By comparison, Lu et al. (2007) estimated changes in MAT and MAP in Weinan in the southern part of the Chinese Loess Plateau over last 136 ka B.P. using phytolith assemblages. Their estimated values for MAT and MAP during 46–23 ka B.P. were 1–2 °C and 100–150 mm higher than those in the region today. Ning et al. (2008) reconstructed paleorainfall in Weinan and Lantian in Chinese Loess Plateau using the stable carbon isotope compositions of soil organic matter. They obtained estimates of MAP at 33 ka B.P. for both study sites that were >200 mm lower than present conditions.

The difference in inferred MAP for Weinan obtained in the two previous studies can likely be attributed to the use of different proxy indicators, which have different sensitivities to temperature

Table 3
Calculated winter and summer average temperature based on mean tooth enamel $\delta^{18}O_P$ of red deer and buffalo.

Sample No.	Species	[a]Winter $\delta^{18}O_P$ (‰,VSMOW)	[a]Summer $\delta^{18}O_P$ (‰, VSMOW)	[b]Winter $\delta^{18}O_P$ corrected (‰, VSMOW)	[b]Summer $\delta^{18}O_P$ corrected (‰, VSMOW)	[c]Winter $\delta^{18}O_{mw}$ (‰, VSMOW)	[c]Summer $\delta^{18}O_{mw}$ (‰, VSMOW)	[d]Winter T_{air} (Eq. (6)) (°C)	[e]Summer T_{air} (from 2MAT-Winter T) (°C)
LCMD2(5):34	Red deer	+12.6 (n = 1)	+14.4 (n = 1)	+11.7 (n = 1)	+15.3 (n = 1)	−12.2	−9.1	0.7 ± 0.5	15.1 ± 1.1
LCMD2(6):19	Red deer	+13.9 (n = 1)	+19.3 (n = 1)	+11.2 (n = 1)	+22.0 (n = 1)	−12.7	−3.2	0 ± 0.5	23.6 ± 1.2
LCMA2(5):56-3	Buffalo	+12.2 ± 0.4 (n = 4)	+14.6 ± 0.1 (n = 2)	+10.4 ± 0.4 (n = 4)	+16.4 ± 0.1 (n = 2)	−13.4 ± 0.4	−8.1 ± 0.1	−1.0 ± 0.7	12.0 ± 1.2
LCMD2(5):16M1	Buffalo	–	–	–	–	–	–	–	–
LCMD2(5):16M2	Buffalo	+11.3 ± 0.5 (n = 3)	+14.1 (n = 1)	+9.2 ± 0.5 (n = 3)	+16.2 (n = 1)	−14.4 ± 0.5	−8.3	−2.5 ± 0.8	11.3 ± 1.3
LCMD2(5):16M3	Buffalo	+11.4 ± 0.7 (n = 3)	+13.4 ± 0.3 (n = 3)	+9.9 ± 0.7 (n = 3)	+14.9 ± 0.3 (n = 3)	−13.8 ± 0.7	−9.4 ± 0.3	−1.6 ± 1.0	8.4 ± 1.3
LCMD2(7):23-2	Buffalo	+16.0 ± 0.2 (n = 5)	+17.1 ± 0.1 (n = 9)	+15.2 ± 0.2 (n = 5)	+18.0 ± 0.1 (n = 9)	−9.1 ± 0.2	−6.7 ± 0.1	5.3 ± 0.7	21.3 ± 1.4

[a] The mean winter and summer $\delta^{18}O_P$ were respectively calculated based on the lowest and highest values of seasonal $\delta^{18}O_P$ curve from each tooth (as indicated in Fig. 3). The ± on each average stands for actual range.

[b] Winter$\delta^{18}O_P$ corrected = (Summer $\delta^{18}O_P$ + Winter $\delta^{18}O_P$)/2 - (Summer $\delta^{18}O_P$ - Winter $\delta^{18}O_P$)/2d_f; Summer $\delta^{18}O_P$ corrected = (Summer $\delta^{18}O_P$ + Winter $\delta^{18}O_P$)/2 + (Summer $\delta^{18}O_P$ - Winter $\delta^{18}O_P$)/2d_f. Values of d_f are 0.5 for red deer and 0.6 for buffalo.

[c] Winter and summer $\delta^{18}O_{mw}$ were calculated based on winter $\delta^{18}O_P$ corrected and summer $\delta^{18}O_P$ corrected, respectively, using equation (2) for buffalo and equation (3) for red deer.

[d] Winter T_{air} was calculated winter $\delta^{18}O_{mw}$ using equation (6). The ± represents an overall uncertainty that takes the variation in winter $\delta^{18}O_{mw}$ and the uncertainty of equation (6) into consideration.

[e] Summer T_{air} was calculated by subtracting the winter T_{air} from 2MAT (eq. (4)). The ± was obtained according to error propagation equation for the calculation.

and rainfall. The pollen and phytolith assemblages both provide an indication of changes in plant compositions, which tend to represent long-term changes in regional climate. These two proxy indicators also reflect overall environmental conditions and cannot be used to differentiate between the effects of temperature and rainfall. By comparison, paleorainfall reconstructions using the carbon isotope of soil organic matter should be relatively reliable because the $\delta^{13}C$ of terrestrial higher plants is much more responsive to changes in rainfall than temperature (Liu et al., 2005). The work of Ning et al. (2008), therefore, which suggests a dry late MIS 3, is likely more reliable than estimates from the pollen and phytolith assemblages. That said, the inferred rainfall amounts using soil organic matter $\delta^{13}C$ provides only a long-term measure of local conditions due to the limited time resolution of samples from loess-paleosol sections.

The $\delta^{13}C_C$ and $\delta^{18}O_P$ of tooth enamel are independent proxies that can be used to reliably infer rainfall and temperature, respectively, on an inter- or intra-annual basis, depending on sampling resolution. In contrast to the warm and wet conditions during MIS 3 proposed in previous studies (*e.g.*, Li et al., 2003; Lu et al., 2007; Chen and Wu, 2008; Yang et al., 2011; Li et al., 2014), our results indicate a generally colder and drier late MIS 3 at our study location. Such dry conditions are consistent with long-term records inferred from soil organic carbon isotope records for the Chinese Loess Plateau during late MIS 3 (Ning et al., 2008).

Solar insolation intensity and global ice volume are two main forcing factors of Earth's climate. During the late MIS 3, average solar insolation over the summer months (June–August) at 33°N, where the Longquan Cave lies, was slightly higher (~10.1 W/m^2) than today (Berger, 1978; Laskar et al., 2004). This condition should facilitate relatively warm overall conditions in the Northern Hemisphere. That said, millennial-scale abrupt climatic events (i.e., Dansgaard-Oeschger cycles and Heinrich events) were common during the MIS 3 and have been well documented in stalagmite $\delta^{18}O$ records for Central China (Wang et al., 2001). In North China, abrupt climatic events such as Heinrich 1 and 2, characterized by cold and dry conditions, have also been recognized in studies of loess deposits (*e.g.*, Wang et al., 2012).

As aforementioned, the decrease in the inferred temperature from sub-layer 7 to 5 may represent a transition from GIS 5 to it30.8(may)-317.4(r)16.lant8erollow70.7(t8ina)mitd17(hi59itio1.7(s9)-38~/F81Tf21.

Grace Yau (LSIS) is thanked for her technical assistance.

Appendix A. Supplementary data

Supplementary data to this article can be found online at https://doi.org/10.1016/j.quascirev.2021.107222.

References

Amiot, R., Lécuyer, C., Buffetaut, E., Fluteau, F., Legendre, S., Martineau, F., 2004. Latitudinal temperature gradient during the cretaceous upper campanian middle maastrichtian: $\delta^{18}O$ record of continental vertebrates. Earth Planet Sci. Lett. 226, 255–272.

Amiot, R., Wang, X., Lécuyer, C., Buffetaut, E., Boudad, L., Cavin, L., Ding, Z., Fluteau, F., Kellner, A.W.A., Tong, H.Y., Zhang, F., 2010. Oxygen and carbon isotope compositions of middle Cretaceous vertebrates from North Africa and Brazil: ecological and environmental significance. Palaeogeogr. Palaeoclimatol. Palaeoecol. 297, 439–451.

Amiot, R., Wang, X., Zhou, Z., Wang, X.L., Buffetaut, E., Lécuyer, C., Ding, Z., Fluteau, F., Hibino, T., Kusuhashi, N., Mo, J.Y., Suteethorn, V., Wang, Y.Q., Xu, X., Zhang, F.S., 2011. Oxygen isotopes of East Asian dinosaurs reveal exceptionally cold early cretaceous climates. Proceedings of National Academy of Sciences of USA 108, 5179–5183.

Amiot, R., Wang, X., Zhou, Z., Wang, X.L., Lécuyer, C., Buffetaut, E., Fluteau, F., Ding, Z., Kusuhashi, N., Mo, J.Y., Philippe, M., Suteethorn, V., Wang, Y.Q., Xu, X., 2015. Environment and ecology of East Asian dinosaurs during the Early Cretaceous inferred from stable oxygen and carbon isotopes in apatite. J. Asian Earth Sci. 98, 358–370.

Azorit, C., Analla, M., Carrasco, R., Calvo, J.A., Muñoz-Cobo, J., 2002. Teeth eruption pattern in red deer (*Cervus elaphus* hispanicus) in southern Spain. Ann. Biol. 24, 107–114.

Bendrey, R., Vella, D., Zazzo, A., Balasse, M., Lepetz, S., 2015. Exponentially decreasing tooth growth rate in horse teeth: implications for isotopic analyses. Archaeometry 57, 1104–1124.

Berger, A., 1978. Long-term variations of daily insolation and Quaternary climate changes. J. Atmos. Sci. 35, 2362–2367.

Bernard, A., Daux, V., Lécuyer, C., Brugal, J.P., Genty, D., Wainer, K., Gardien, V., Fourel, F., Jaubert, J., 2009. Pleistocene seasonal temperature variations recorded in the $\delta^{18}O$ of Bison priscus teeth. Earth Planet Sci. Lett. 283, 133–143.

Bonafini, M., Pellegrini, M., Ditchfield, P., Pollard, A.M., 2013. Investigation of the 'canopy effect' in the isotope ecology of temperate woodlands. J. Archaeol. Sci. 40, 3926–3935.

Brown, W.A.B., Chapman, N.G., 1991. Age assessment of red deer (*Cervus elaphus*): from a scoring scheme based on radiographs of developing permanent molariform teeth. J. Zool. 225, 85–97.

Bryant, J.D., Luz, B., Froelich, P.N., 1994. Oxygen isotopic composition of fossil horse tooth phosphate as a record of continental paleoclimate. Palaeogeogr. Palaeoclimatol. Palaeoecol. 107, 303–316.

Bryant, D., Froelich, P., Showers, W., Genna, B., 1996. Biologic and climatic signals in the oxygen isotopic composition of Eocene–Oligocene equid enamel phosphate. Palaeogeogr. Palaeoclimatol. Palaeoecol. 126, 75–89.

Cerling, T.E., Harris, J., MacFadden, B., Leakey, M., Quade, J., Eisenmann, V., Ehleringer, J., 1997. Global vegetation change through the Miocene–Pliocene boundary. Nature 389, 153–158.

Cerling, T.E., Harris, J.M., 1999. Carbon isotope fractionation between diet and bioaptite in ungulate mammals and implications for ecological and paleoecological studies. Oecologia 120, 347–363.

Chappell, J., 2002. Sea level changes forced ice breakouts in the Last Glacial Cycle: new results from coral terraces. Quat. Sci. Rev. 21, 1229–1240.

Chen, X.Y., Wu, N.Q., 2008. Relatively warm-humid climate recorded by mollusk species in the Chinese Loess Plateau during MIS 3 and its possible forcing mechanism. Quat. Sci. 28, 154–161 (In Chinese with English abstract).

Compilatory Commission of Annals of Luanchuan County, 1994. In: Annals of Luanchuan County. SDX Joint Publishing Company, Beijing, pp. 74–77.

Coplen, T.B., Kendall, C., Hopple, J., 1983. Comparison of stable isotope reference samples. Nature 302, 236–238.

Cormie, A.B., Luz, B., Schwarcz, H.P., 1994. Relationship between the hydrogen and oxygen isotopes of deer bone and their use in the estimation of relative humidity. Geochem. Cosmochim. Acta 58, 3439–3449.

Crowson, R.A., Showers, W.J., Wright, E.K., Hoering, T.C., 1991. A method for preparation of phosphate samples for oxygen isotope analysis. Anal. Chem. 63, 2397–2400.

D'Angela, D., Longinelli, A., 1990. Oxygen isotopes in living mammal's bone phosphate: further results. Chem. Geol. 86, 75–82.

Dansgaard, W., 1964. Stable isotopes in precipitation. Tellus 16, 436–468.

Dansgaard, W., Johnsen, S., Clausen, H.B., Dahl-Jensen, D., Gundestrup, N., Hammer, C.U., Oeschger, H., 1984. North Atlantic climatic oscillations revealed by deep Greenland ice cores. In: Hansen, J.E., Takahashi, T. (Eds.), Climate Processes and Climate Sensitivity. American Geophysical Union, Washington, pp. 288–298.

Dansgaard, W., Johnsen, S.J., Clausen, H.B., Dahl-Jensen, D., Gundestrup, N.S., Hammer, C.U., Hvidberg, C.S., Steffensen, J.P., Sveinbjörnsdottir, A.E., Jouzel, J., Bond, G., 1993. Evidence for general instability of past climate from a 250-kyr ice-core record. Nature 364, 218–220.

Deines, P., 1980. The isotopic composition of reduced organic carbon. In: Fritz, P., Fontes, J.C. (Eds.), Handbook of Environmental Isotope Geochemistry. Elsevier, Amsterdam, pp. 329–406.

Delgado Huertas, A., Iacumin, P., Longinelli, A., 1997. A stable isotope study of fossil mammal remains from the Paglicci cave, southern Italy, 13 to 33 ka BP: palaeoclimatological considerations. Chem. Geol. 141, 211–223.

Deng, T., Dong, J., Wang, Y., 2002. Variation of terrestrial ecosystem recorded by stable carbon isotopes of fossils in northern China during the Quaternary. Chin. Sci. Bull. 47 (1), 76–78.

Deng, T., Li, Y.M., 2005. Vegetational ecotype of the Gyirong Basin in Tibet, China and its response in stable carbon isotopes of mammal tooth enamel. Chin. Sci. Bull. 50 (12), 1225–1229.

Dettman, D.L., Kohn, M.J., Quade, J., Ryerson, F.J., Ojha, T.P., Hamidullah, S., 2001. Seasonal stable isotope evidence for a strong Asian monsoon throughout the past 10.7 m.y. Geology 29, 31–34.

Drucker, D.G., Bridault, A., Hobson, K.A., Szuma, E., Bocherens, H., 2008. Can carbon-13 in large herbivores reflect the canopy effect in temperate and boreal ecosystems? Evidence from modern and ancient ungulates. Palaeogeogr. Palaeoclimatol. Palaeoecol. 266, 69–82.

Du, S.S., Li, X., Zhou, L., Pang, H.J., Bar-Yosef, O., Wu, X.H., 2016. Longquan cave: an early upper palaeolithic site in henan province, China. Antiquity 90, 876–893.

Fabre, M., Lécuyer, C., Brugal, J.-P., Amiot, R., Fourel, F., Martineau, F., 2011. Late Pleistocene climatic change in the French Jura (Gigny) recorded in the $\delta^{18}O$ of phosphate from ungulate tooth enamel. Quat. Res. 75, 605–613.

Faegri, K., Kaland, P.E., Krzywinski, K., 1989. In: Textbook of Pollen Analysis, fourth ed. John Wiley & Sons, London, pp. 1–328.

Farquhar, G., Ehleringer, K., Hubick, K., 1989. Carbon isotope discrimination and photosynthesis. Annu. Rev. Plant Physiol. Plant Mol. Biol. 40, 503–537.

Flanagan, L.B., Farquhar, G.D., 2014. Variation in the carbon and oxygen isotope composition of bioma-428Tf6.630.1(Ki)21(ope)ordpe9(change)-0raeth5-430.4(cl(.)-5ant)-.6

compositions: effects of diet and physiology. Geochem. Cosmochim. Acta 60, 3889–3896.
Kohn, M.J., Cerling, T.E., 2002. Stable isotope compositions of biological apatite. In: Kohn, M., Rakovan, J., Hughes, J. (Eds.), Phosphates—Geochemical, Geobiological, and Materials Importance. Reviews in Mineralogy and Geochemistry, vol. 48. Mineralogical Society of America, Washington D.C., pp. 455–488
Kohn, M.J., 2004. Comment: tooth enamel mineralization in ungulates: implications for recovering a primary isotopic time-series, by B.H. Passey and T.E. Cerling (2002). Geochem. Cosmochim. Acta 68, 403–405.
Laskar, J., Robutel, P., Joutel, F., Gastineau, M., Correia, A.C.M., Levrard, B., 2004. A long-term numerical solution for the insolation quantities of the Earth. Astron. Astrophys. 428, 261–285.
Lécuyer, C., Grandjean, P., O'Neil, J.R., Cappetta, H., Martineau, F., 1993. Thermal excursions in the ocean at the Cretaceous-Tertiary boundary (northern Morocco): $\delta^{18}O$ record of phosphatic fish debris. Palaeogeogr. Palaeoclimatol. Palaeoecol. 105, 235–243.
Li, Y.M., Liu, T.S., Wu, W.X., Han, J.M., Hong, Y.T., 2003. Paleoenvironment in Chinese Loess Plateau during MIS 3: evidence from malan loess. Quat. Sci. 23, 69–76 (In Chinese with English abstract).
Li, Y.S., Chen, J.Q., Zhao, S., Wang, H.Y., Li, X., 2011. Quantitative reconstruction of palaeoclimate since 200 ka BP in Tangshan area, Hebei Province. Mar. Geol. Quat. Geol. 31, 163–170 (In Chinese with English abstract).
Li, X.Q., Gao, Q., Hou, Y.M., Zhao, K.L., Sun, N., Yang, Z.M., Zhen, Z.M., Liu, Y., Zhou, X.Y., 2014. The vegetation and environment at the Wulamulun site in the Ordos Plateau, Inner Mongolia during MIS 3 period. Acta Anthropol. Sin. 33, 60–69.
Liu, W.G., Feng, X.H., Ning, Y.F., Zhang, Q.L., Cao, Y.N., 2005. $\delta^{13}C$ variation of C_3 and C_4 plants across an Asian monsoon rainfall gradient in arid northwestern China. Global Change Biol. 11, 1094–1100.
Longinelli, A., 1984. Oxygen isotopes in mammal bone phosphate: a new tool for paleohydrological and paleoclimatological research? Geochem. Cosmochim. Acta 48, 385–390.
Lourantou, A., Lavric, J.V., Köhler, P., Barnola, J.-M., Paillard, D., Michel, E., Raynaud, D., Chappellaz, J., 2010. Constraint of the CO_2 rise by new atmospheric carbon isotopic measurements during the last deglaciation. Global Biogeochem. Cycles 24, GB2015. https://doi.org/10.1029/2009GB003545.
Lu, H.Y., Wu, N.Q., Liu, K.B., Jiang, H., Liu, T.S., 2007. Phytoliths as quantitative indicators for the reconstruction of past environmental conditions in China II: palaeoenvironmental reconstruction in the Loess Plateau. Quat. Sci. Rev. 26, 759–772.
Luz, B., Kolodny, Y., Horowitz, M., 1984. Fractionation of oxygen isotopes between mammalian bone-phosphate and environmental drinking water. Geochem. Cosmochim. Acta 48, 1689–1693.
MacFadden, B., Cerling, T., Prado, J., 1996. Cenozoic terrestrial ecosystem evolution in Argentina: evidence from carbon isotopes of fossil mammal teeth. Palaios 11, 319–327.
Maher, L.J., 1981. Statistics for microfossil concentration measurements employing samples spiked with marker grains. Rev. Palaeobot. Palynol. 32, 153–191.
Marino, B.D., McElroy, M.B., Salawitch, R.J., Spaulding, W.G., 1992. Glacial-to-interglacial variations in the carbon isotopic composition of atmospheric CO_2. Nature 357, 461–466.
Metcalfe, J.Z., Longstaffe, F.J., Ballenger, J.A.M., Vance Haynes Jr., C., 2011. Isotopic paleoecology of Clovis mammoths from Arizona. Proceedings of National Academy of Sciences of USA 108 (44), 17916–17920.
Moss-Salentijn, L., Moss, M.L., Yuan, M.S., 1997. The ontogeny of mammalian enamel. In: Koeningswald, W.V., Sander, P.M. (Eds.), Tooth Enamel Microstructure. A. A. Balkema, pp. 5–30.
Ning, Y.F., Liu, W.G., An, Z.S., 2008. A 130-ka reconstruction of precipitation on the Chinese Loess Plateau from organic carbon isotopes. Palaeogeogr. Palaeoclimatol. Palaeoecol. 270, 59–63.
O'Leary, M.H., 1981. Carbon isotope fractionation in plants. Phytochemistry 20, 553–567.
O'Leary, M.H., 1988. Carbon isotopes in photosynthesis. Bioscience 38, 328–336.
Passey, B.H., Cerling, T.E., 2002. Tooth enamel mineralization in ungulates: implications for recovering a primary isotopic time-series. Geochem. Cosmochim. Acta 66, 3225–3234.
Passey, B.H., Robinson, T.F., Ayliffe, L.K., Cerling, T.E., Sponheimer, M., Dearing, M.D., Roeder, B.L., Ehleringer, J.R., 2005. Carbon isotope fractionation between diet, breath CO_2, and bioapatite in different mammals. J. Archaeol. Sci. 32, 1459–1470.
Pellegrini, M., Snoeck, C., 2016. Comparing bioapatite carbonate pre-treatments for isotopic measurements: Part 2- Impact on carbon and oxygen isotope compo-

Plateau. Earth Planet Sci. Lett. 236, 322–338.
Wang, Y.J., Lv, H.Y., Wang, G.A., Yang, H., Li, Z., 2000. Carbon isotope analysis of silicates in C3, C4 plants and modern soils. Chin. Sci. Bull. 45, 978–982 (In Chinese).
Wang, Y.J., Cheng, H., Edwards, R.L., An, Z.S., Wu, J.Y., Shen, C.-C., Dorale, J.A., 2001. A high-resolution absolute-dated late Pleistocene monsoon record from Hulu Cave, China. Science 294, 2345–2348.
Webb, E.C., White, C.D., Longstaffe, F.J., 2014. Investigating inherent differences in isotopic composition between human bone and enamel bioapatite: implications for reconstructing residential histories. J. Archaeol. Sci. 50, 97–107.
Wu, H., Hou, W., Qian, Z.H., Hu, J.G., 2012. The research on the sensitivity of climate change in China in recent 50 years based on composite index. Acta Phys. Sin. 61 (14), 149205.
World Data Center for Paleoclimatology, 2006. Boulder and NOAA Paleoclimatology program [DB/OL]. http://hurricane.ncdc.noaa.gov/pls/paleox/f?p=519:1:::::P1_STUDY_ID:9972.
Yang, Q., Li, X.Q., Zhou, X.Y., Liu, H.H., Zhao, K.L., Sun, N., 2011. Vegetation succession and its response to climate changes since MIS 3 in desert-loess transition belt, Northern China. Quat. Sci. 31 (6), 962–971 (In Chinese with English abstract).
Yang, S.L., Ding, Z.L., 2008. Advance-retreat history of the East-Asian summer monsoon rainfall belt over northern China during the last two glacial–interglacial cycles. Earth Planet Sci. Lett. 274, 499–510.
Yang, S.L., Ding, Z.L., Wang, X., Tang, Z.H., Gu, Z.Y., 2012. Negative $\delta^{18}O$-$\delta^{13}C$ relationship of pedogenic carbonate from northern China indicates a strong response of C3/C4 biomass to the seasonality of Asian monsoon precipitation. Palaeogeogr. Palaeoclimatol. Palaeoecol. 317/318, 32–40.
Zazzo, A., Balasse, M., Patterson, W.P., 2005. High-resolution $\delta^{13}C$ intratooth profiles in bovine enamel: implications for mineralization pattern and isotopic attenuation. Geochem. Cosmochim. Acta 69, 3631–3642.
Zazzo, A., Balasse, M., Passey, B.H., Moloney, A.P., Monahan, F.J., Schmidt, O., 2010. The isotope record of short- and long-term dietary changes in sheep tooth enamel: implications for quantitative reconstruction of paleodiets. Geochem. Cosmochim. Acta 74, 3571–3586.
Zhao, Z.J., 1974. Red deer's living habits and its capture method. Chin. J. Zool. 9 (1), 22–23 (In Chinese).